Desalination and Water Treatment
www.deswater.com

doi: 10.5004/dwt.2023.29649

297 (2023) 102–116
June

Removal of lead ions and bisphenol S using β-cyclodextrin modified peanut shell from solution

Yang Liu, Yuanyuan Wang, Jie Ma, Runping Han*

College of Chemistry, Zhengzhou University, No. 100 of Ke xue Road, Zhengzhou, 450001, China, emails: rphan67@zzu.edu.cn (R.P. Han), g1836b@163.com (Y. Liu), 2305942027@qq.com (Y.Y. Wang), monica105@qq.com (J. Ma)

Received 3 February 2023; Accepted 16 May 2023

ABSTRACT

In this study, peanut shell was modified using β-cyclodextrin (β-CD) and citric acid to improve the adsorption capacity for removal of lead ion (Pb^{2+}) and bisphenol S (BPS) from solution in batch mode. Scanning electron microscopy, Fourier-transform infrared spectroscopy, elemental analysis, X-ray fluorescence analysis, specific surface area analysis, thermogravimetric analysis, etc were used to characterize the adsorbent before and after modification. The results showed that the adsorbent was successfully modified. The adsorption results of Pb^{2+} and BPS on β-CD-PS indicated that acidic conditions were not conducive to the adsorption of Pb^{2+}, the adsorption of BPS basically remained unchanged at pH 2~7, and alkaline conditions were not conducive to the adsorption. The presence of salt had a negative effect on Pb^{2+}, but had no effect on the adsorption of BPS. The Langmuir and Koble–Corrigan models could predict the equilibrium adsorption process of Pb^{2+} while Temkin and Koble–Corrigan models could describe the equilibrium adsorption process of BPS. The adsorption quantity from experiments is 89.6 $mg \cdot g^{-1}$ for Pb^{2+} and 16.2 $mg \cdot g^{-1}$ for BPS at 293 K, respectively. The adsorption process of Pb^{2+} was consistent with the pseudo-first-order and Elovich models, indicating the presence of ion-exchange in the adsorption process; the adsorption of BPS was consistent with the pseudo-second-order model, indicating that chemisorption was the main rate-controlling step. Thermodynamic studies indicated that the adsorption of Pb^{2+} was a spontaneous and endothermic reaction with increasing entropy, while the adsorption of BPS was a spontaneous and exothermic reaction with decreasing entropy. 0.1 $mol \cdot L^{-1}$ HNO_3 could desorb and regenerate the β-CD-PS adsorbed Pb^{2+} for three times, and 75% C_2H_5OH had a better desorption and regeneration effect for BPS loaded β-CD-PS. β-CD-PS can effectively remove the lead ion and BPS from mixtures and the study can provide the basis for the effective utilization of peanut shell in environmental remediation.

Keywords: Adsorption; β-cyclodextrin modified peanut shell; Lead ion; Bisphenol S; Regeneration

1. Introduction

Water is one of the most abundant substances on earth and is essential for human functions [1], however, with the rapid socio-economic development and the expanding population size in China, the industrialization process is accelerating the continuous production in order to cope with the increasing demand of various basic products, which eventually leads to many harmful wastewater discharged into the environment without any treatment, resulting in serious pollution [2], and currently, the sources of water pollution were mining, paper, textile, plastic, leather, paint, dyes, pesticides, agricultural fertilizers etc [3,4]. The generation of these harmful wastewaters can potentially harm the ecological environment and human health [5–7], so we need effective measures to improve the water pollution problem.

* Corresponding author.

Lead is one of the five toxic heavy metals with high toxicity. It is mainly used as a pigment, insecticide, fertilizer and gasoline additive [8]. Low concentration of lead has a great impact on human health and aquatic organisms. Long-term accumulation of lead through food can lead to respiratory diseases, weakened immune system, kidney or liver damage, genetic and nervous system changes and death [9,10]. In order to monitor environmental pollution and protect human health, the World Health Organization has set the maximum allowable concentration of lead in drinking water as 0.01 $mg \cdot L^{-1}$ [11]. Therefore, it is necessary to use effective methods to reduce the content of lead in water to avoid its harm to human body and environment.

Bisphenol S (BPS) is one of the common alternatives to bisphenol A (BPA) used in various industrial applications, including polycarbonate plastics, PVC, food packaging, dental sealants, dye dispersants, and fiber modifiers [12–14]. The increase of BPS leads to relatively large environmental load and potential negative impact on the ecosystem [15]. Several recent studies have shown that BPS has a variety of adverse reactions, including cytotoxicity, genotoxicity, immunotoxicity and REDOX toxic effects in humans and animals [16], and BPS can induce endocrine diseases and has a great impact on the nervous system [17]. Therefore, the removal of bisphenol S from water is very important to the ecological environment and human health.

β-cyclodextrin (β-CD) is a cyclic oligosaccharide composed of seven D-glucopyranose units, forming a dome-like molecular structure, which is an environmentally friendly and inexpensive adsorbent [18]. β-CD has a special structure of hydrophilic outer surface and hydrophobic inner cavity. Based on the hydrophobic interaction between organic chemicals and β-CD inner cavity, guest-guest complex can be formed. Therefore, β-CD has great potential to remove hydrophobic organic pollutants from water. However, since β-CD is easily soluble in water and difficult to separate, more and more studies have been conducted on its modification to improve its practical application in removing organic pollutants from water [19]. Cyclodextrin polymers have been prepared using cross-linking, which not only introduces some special functional groups but also imparts a three-dimensional structure to the adsorbent. Therefore, the performance of cyclodextrin polymerized by crosslinking is usually superior to that of the parent cyclodextrin [20]. Zhou et al. [21] prepared cyclodextrin polymer (β-CDP), whose maximum adsorption capacities for BPA, chlorophenol (PCMX) and carbamazepine (CBZ) were 164.4, 144.1 and 136.4 $mg \cdot g^{-1}$, respectively.

The water environment has become polluted due to the large amount of wastewater containing toxic pollutants (such as dyes, heavy metals, surfactants, personal care products, pesticides and pharmaceuticals) flowing into rivers from agricultural, industrial and municipal sources. Water pollution and its treatment has become a growing challenge worldwide. In recent years, great efforts have been made to overcome the challenges of wastewater treatment. Current methods of wastewater treatment include chemical methods (e.g., electrochemical oxidation [22], chemical precipitation [23], and ion-exchange [24,25]), physical methods (e.g., membrane filtration [26]), physico-chemical methods (e.g., adsorption), and some biotechnologies [27]. Among these methods, physical methods mainly remove some large particle pollutants; chemical methods were costly and complicated to operate; and adsorption methods were widely used because of their simple operation and low cost [28].

Due to the high price and poor regeneration of traditional biosorbents, more and more researchers are focusing on new energy sources such as biomass [29,30]. Biomass is also known as agricultural and forestry waste, which is a by-product of agricultural and forestry production and some processing enterprises [31]. They are widely available, inexpensive, renewable, and less polluting to the environment. The main biomass adsorbents are wheat straw [32], rice husk [33], corn cob [34,35], bagasse [36], walnut shell [37], peanut shell [38], wood chips [39], and leaves [40,41]. Zhao et al. [42] modified wheat straw with cationic surfactants to remove Congo red from water and obtained a relatively good adsorption effect. Therefore, in the present experiment we used peanut shells as the basis for the adsorbent.

In the study, β-CD-PS was prepared and characterized, and its adsorption properties toward Pb^{2+} and BPS in solution were also presented. The process was evaluated by kinetic, equilibrium and thermodynamic analyses, and the performance of β-CD-PS about desorption and regeneration after the adsorption of Pb^{2+} and BPS was investigated.

2. Materials and methods

2.1. Materials

2.1.1. Experimental materials

Peanut shells (from Yanshi District, Luoyang City, Henan Province, China) were crushed and screened, and peanut shells with diameter of 40–60 mesh were collected, soaked and cleaned with deionized water for many times, and dried at 80°C for later use.

2.1.2. Experimental reagent

Ethanol was purchased from Xinxiang Sanwei Disinfection Preparation Co., Ltd., (China), β-cyclodextrin (β-CD) was purchased from Tianjin Kemiou Chemical Reagent Co., Ltd., (China), citric acid (CA) was purchased from Tianjin Fuchen Chemicals Reagent Factory (China), sodium hypophosphite ($NaH_2PO_2 \cdot H_2O$) was provided by Tianjin Kemiou Chemical Reagent Co., Ltd., (China), Tianjin Fucheng Chemical Reagent Factory (China) provided sodium hydroxide (NaOH) and sodium chloride (NaCl), hydrochloric acid (HCl) from Yantai Shuangshuang Chemical Co., Ltd., (China), anhydrous calcium chloride ($CaCl_2$) from Tianjin Yongda Chemical Reagent Co., Ltd., (China), bisphenol sulfur (BPS) from Shanghai Aladdin Biochemical Technology Co., Ltd., (China), lead nitrate ($Pb(NO_3)_2$) was purchased from Tianjin Kemiou Chemical Reagent Co., Ltd., (China). Deionized water was made by ourselves as experimental water. All chemicals were analytical grade.

2.1.3. Experimental instruments

The digital display water bath constant temperature oscillator was purchased from Changzhou Putian Instrument

Manufacturing Co., Ltd., (China), the electric blast drying oven was purchased from Shanghai Yiheng Scientific Instrument Co., Ltd., (China), the analytical balance was purchased from Shanghai Shangping Instrument Co., Ltd., (China), the precision acid meter was purchased from Shanghai Yiheng Scientific Instrument Co., Ltd., (China), the pulverizer was purchased from Shanghai Jiarui Tool Co., Ltd., (China), the peristaltic pump was purchased from Lange Constant Current Pump Co., Ltd., (China), Ningbo Xinzhi Biotechnology Co., Ltd., (China), UV-visible spectrophotometer purchased from Shanghai Shunyu Hengping Instrument Co., Ltd., (China), flame atomic absorption spectrophotometer purchased from Beijing East-West analysis, Fourier-transform infrared spectrometer purchased from the United States PE Company. The elemental analyzer was purchased from Thermo Electron Corporation and the scanning electron microscope was purchased from FEI, The Netherlands.

2.2. Prepare of cyclodextrin modified peanut shells

The peanut shells were immersed in 5% NaOH (1:5) solution, oscillated at 50°C in a constant temperature oscillator for 4 h, removed and filtered, washed to neutral with distilled water and ethanol, and dried at 80°C for 12 h to obtain the peanut shells (NPS) after alkali treatment. The peanut shells treated with 2 g alkali were placed in a 100 mL beak, with 2 g sodium hypophosphite, 3 g citric acid, 3 g β-cyclodextrin and 70 mL H_2O. The shells were ultrasound at 80°C for 20 min to fully dissolve. The shells were reacted in an oven at 180°C for 70 min, then washed in distilled water until neutral and dried. β-cyclodextrin modified peanut shell adsorbent was prepared, which was called β-CD-PS.

2.3. Characterization of cyclodextrin modified peanut shells

The adsorbent β-CD-PS was characterized to study the structure and properties of the adsorbent before and after modification, and further study its adsorption mechanism. The characterization methods used in this paper include scanning electron microscopy, Fourier-transform infrared spectroscopy analysis, elemental analysis, specific surface area analysis, thermogravimetric analysis (TG) and isoelectric point determination.

The following process was to determine the isoelectric point. Taking a series of 50 mL conical bottles, added 10 mL 0.01 mol·L^{-1} NaCl solution, adjusted the pH value of the solution between 1.00 and 12.00, add 0.010 mg modified material, shook in a constant temperature oscillation chamber for 313 K for 12 h, filtered and separated. The pH value of NaCl solution after oscillation was measured. The initial pH value of the solution was taken as the abscissa, and the change of pH value before and after oscillation was taken as the ordinate. The intersection point between the curve and the abscissa was the isoelectric point of the adsorbent.

2.4. Method for the determination of pollutant content

The determination methods of Pb^{2+} and BPS were as follows: Pb^{2+} with a wavelength of 283.3 nm was detected by flame atomic absorption spectrophotometry; BPS with a wavelength of 259 nm was detected by UV-VIS spectrophotometry. When pH was determined, standard solution correction was performed by potentiometric analysis.

2.5. Adsorption experiments

The adsorption test was performed in batch mode. A certain mass of adsorbent (such as 10 mg) was put into 50 mL conical flask and 10 mL of Pb^{2+} (such as 200 mg·L^{-1}) or BPS solution (such as 50 mg·L^{-1}) was added. The effects of temperature (293, 303 and 313 K), adsorbate concentration and time, solution pH and salinity on the adsorption of Pb^{2+} and BPS were investigated. Filtration was used to separate the solids from the mixtures. The concentration of Pb^{2+} or BPS was measured, and the unit adsorption quantity q and removal efficiency (p, %) were calculated by Eqs. (1) and (2).

$$q = \frac{V\left(C_0 - C\right)}{m} \tag{1}$$

$$p = \frac{C_0 - C}{C_0} \times 100\% \tag{2}$$

where q is the unit adsorption amount (mg·g^{-1}), V is the volume of adsorbent solution (L), C_0 is the initial concentration of adsorbent (mg·L^{-1}), C is the residual concentration after adsorption (mg·L^{-1}), m is the mass of adsorbent (g), and p is the removal rate (%).

2.6. Desorption study

This part was focused on batch desorption and regeneration. Firstly, weigh 0.010 g of β-CD-PS, add to 10 mL 200 mg·L^{-1} Pb^{2+} solution or 50 mg·L^{-1} BPS solution, respectively, sealed and shaken at 303 K until equilibrium. After this, the material was washed with distilled water, dried. Then the spent adsorbent was desorbed or regenerated using several methods. The spent adsorbent was regenerated and the desorption efficiency (d) and regeneration rate (r) were calculated. Then the unit adsorption quantity q_m and the mass m_0 of adsorbate were measured and calculated. With distilled water to wash the adsorbent to neutral, drying, adsorption performance was repeated and the unit adsorption quantity q_r was calculated. The solution with the best efficiency of desorption and regeneration was selected for multiple desorption and regeneration. The desorption efficiency (d, %) and regeneration efficiency (r, %) could be calculated by Eqs. (3) and (4).

$$d = \frac{m_d}{m_0} \times 100\% \tag{3}$$

$$r = \frac{q_r}{q_m} \times 100\% \tag{4}$$

3. Results and discussion

3.1. Characterization of materials

In order to study the changes of surface characteristics of peanut shell before and after modification, scanning

electron microscope analysis was conducted on the peanut shell before and after modification, and the results were shown in Fig. 1b.

As can be seen from Fig. 1, the surface structure of peanut shell before modification was tight and irregular. As can be seen from Fig. 1b, the surface of β-CD-PS presented a regular fibrous structure, indicating the successful modification of peanut shell.

Fig. 1c indicates the infrared spectrum of NPS and β-CD-PS. The peak at 1,738 cm^{-1} was ascribed to the stretching vibration of C=O. The strong peak at 1,265 cm^{-1} was due to the asymmetric stretching vibration peak of C–O–C while the absorption at 1,421 cm^{-1} was due to the symmetric stretching vibration of C–O–C, indicating that the material contained ester groups. For β-CD-PS, the hydroxyl peak at 3,440 cm^{-1} was wide and strong, and the peak from C=O was also stronger, indicating that the number of carboxyl groups on the material became more and the material was successfully modified.

Element analysis was carried out to explore the changes of element content in peanut shell before and after modification. There was 0.310% for N, 51.0 for C, 5.74% for H about not modified peanut shell or natural peanut shell (NPS) and 0.290% for N, 53.8% for C, 6.88% for H about β-CD-PS. The content of C and H in β-CD-PS was higher than those in NPS, indicating that some new groups have been introduced.

The specific surface area of β-CD-PS was 0.139 $m^2 \cdot g^{-1}$ while it was 0.925 $m^2 \cdot g^{-1}$ for NPS. The specific surface area of PS decreases after modification, which may be caused by alkali treatment and surface graft functional groups during modification.

Fig. 1d indicates the thermogravimetric analysis of peanut shell before and after modification. It can be seen from Fig. 1d that the weight lost of peanut shell was divided into several stages with the rise of temperature. Peanut shell contained a large number of cellulose, its molecular chain contained a large number of hydrophilic groups hydroxyl, which can absorb water molecules and small molecules in the air. The first stage was preheating and holding, and the temperature range was 20°C~250°C. In this stage, the TG line was relatively stable, and the peanut shell basically has no change in weight loss. The second stage was thermal decomposition, the temperature range was 250°C~500°C, mainly the side chain and partial oxygen bridge bond of benzene ring in peanut shell cellulose, hemicellulose and lignin fracture. The temperature ranges from 250°C to 320°C, the weight lost rate was 30.9%, mainly due to the decomposition of cellulose and hemicellulose. The temperature range was 320°C~510°C, the weight lost rate was 59.1%, mainly due to the decomposition of lignin. The temperature range was 510°C~1,050°C, the mass of this stage remains unchanged, mainly some inorganic salts. Compared with PS, the weightlessness in β-CD-PS was similar to that of natural peanut shells.

The isoelectric point of adsorbent before and after modification is shown in Fig. 2a and b.

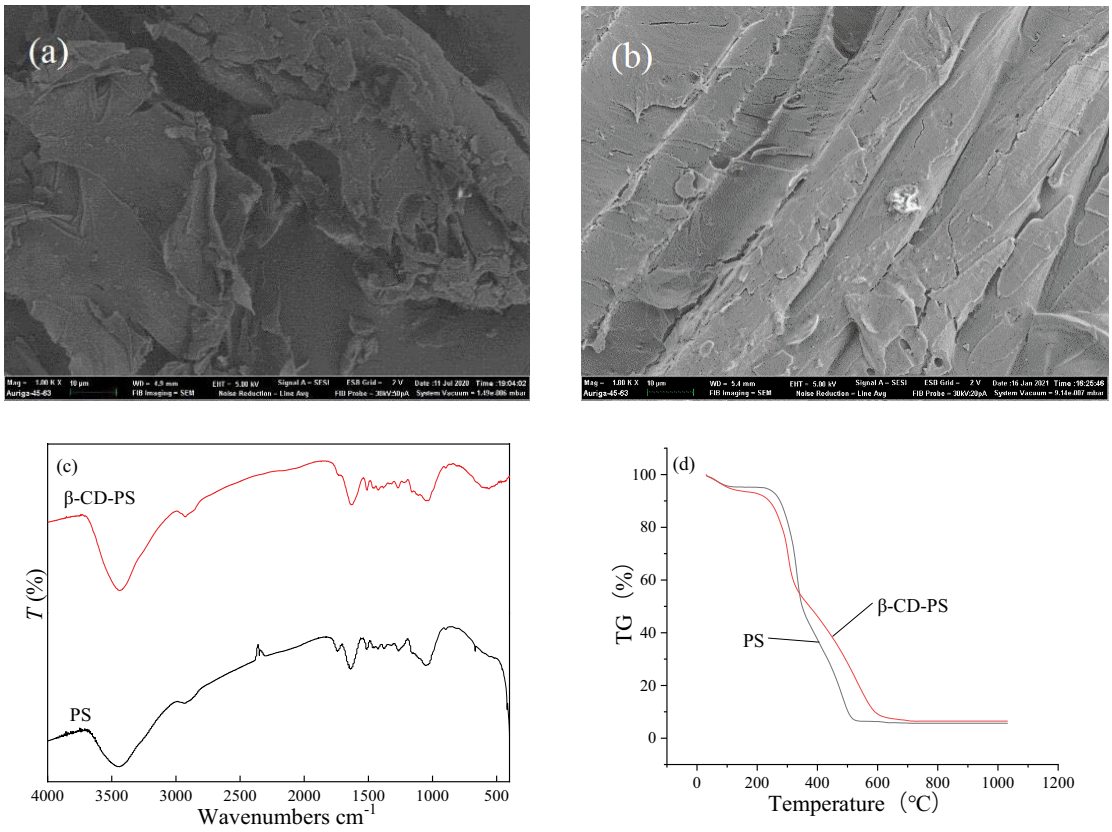

Fig. 1. Scanning electron micrograph of shell of peanut (a) and β-CD-PS (b), Fourier-transform infrared spectroscopy of NPS and β-CD-PS (c), thermogravimetric analysis curve of NPS and β-CD-PS (d).

Fig. 2a shows that the isoelectric point of NPS is 5.82. Fig. 2b shows that isoelectric point of β-CD-PS is 3.70. The modified materials had different degrees of influence on the equivalent electrical point. The isoelectric point of β-CD-PS moved towards acidity because the carboxyl group of citric acid was introduced to make its isoelectric point smaller.

3.2. Adsorption study

3.2.1. Comparative studies of adsorption capacities of Pb^{2+} and BPS on various materials

For assess the value of modification, adsorption capacity before and after modification is compared. 10 mg of NPS or β-CD-PS was added in the conical bottles containing 10 mL Pb^{2+} solution of 200 mg·L^{-1} or BPS solution of 50 mg·L^{-1}. The values of q_e about NPS were 3.60 mg·g^{-1} for Pb^{2+} and 0.720 mg·g^{-1} for BPS while the values of q_e about β-CD-PS were 90.6 mg·g^{-1} for Pb^{2+} and 5.95 mg·g^{-1} for BPS, respectively. This confirmed that the adsorption capacity of the modified material was significantly increased under the same adsorption conditions, indicating that the modified material was successful valuable.

3.2.2. Effect of adsorbent dose on adsorption

Adsorbent dose was also effective to remove adsorbates from solution. The effect of adsorbent dose on adsorption is shown in Fig. 2c and d. The results showed that the amount of adsorbent was inversely proportional to the unit adsorption amount and proportional to the removal efficiency. In Fig. 2c, with the increase of adsorbent mass, the values of q_e decreased from 132 to 79.0 mg·g^{-1} while the values of p increased from 12.6% to 79.0%. In Fig. 2d, with the increase of adsorbent mass, the value of q_e decreased from 8.64 to 5.49 mg·g^{-1}, and the values of p increased from 3.70% to 21.3%. This was because when the mass of the adsorbent was low, there were fewer active sites that could be adsorbed, the removal rate was low, the amount of adsorbent was certain, and the unit active site could be combined with more adsorbent [43]. When the mass of adsorbent was large, the adsorbent could be adsorbed more sites, the removal rate was high, but the average unit active site can bind less adsorbent mass, the unit adsorption capacity was low. Lv et al. [44] also had similar results on the adsorption of BPS. Considering the adsorption capacity and removal rate, the mass of adsorbent selected in the subsequent experiments was 0.010 g.

3.2.3. Effect of pH on adsorption

Solution pH often played important role in adsorption process as pH could affect the existed form of adsorbate and surface property of adsorbent. Fig. 3 shows the results of solution pH on adsorption. Through Fig. 3a and b, the results showed that acidic conditions were not conducive to the adsorption of Pb^{2+} on β-CD-PS, which may be because the presence of H^+ competes with Pb^{2+} when pH was relatively low, resulting in the decrease of adsorption capacity.

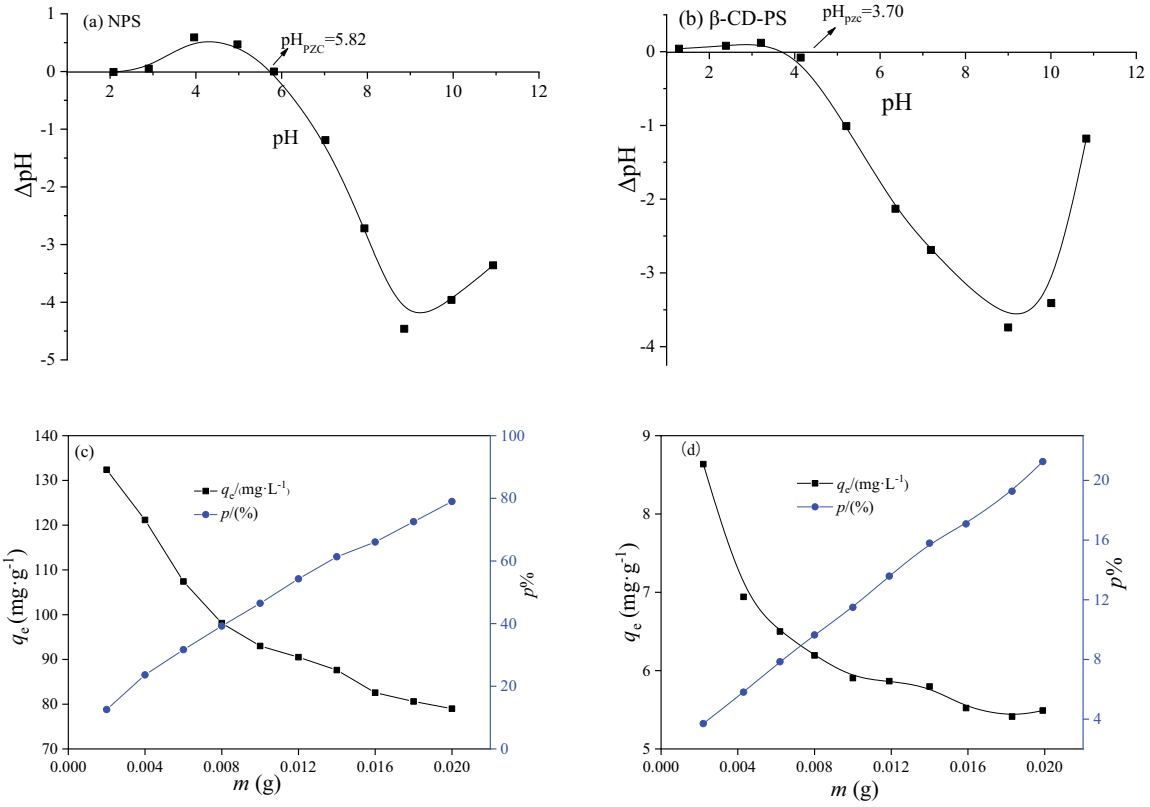

Fig. 2. Isoelectric plot of PS (a) and β-CD-PS; effect of adsorbent dosage on adsorption of Pb^{2+} (c) and BPS (d).

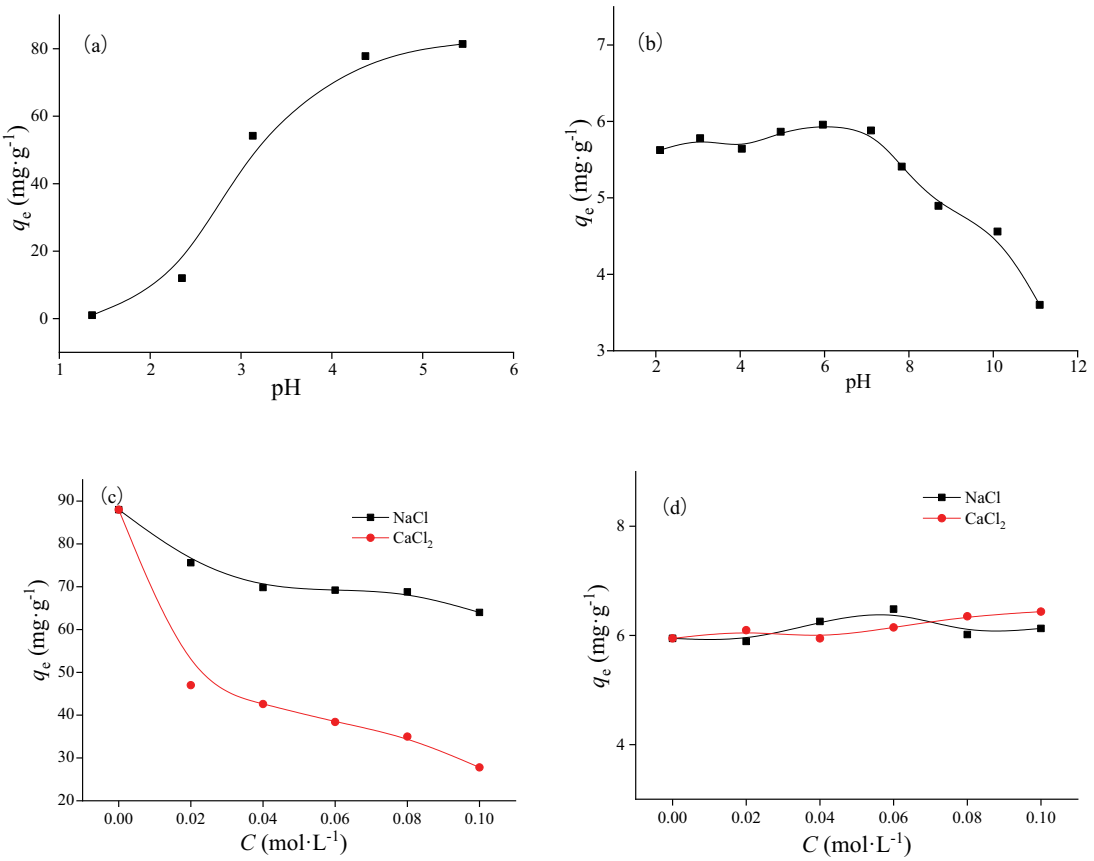

Fig. 3. Effect of pH on adsorption of Pb^{2+} (a) and BPS on β-CD-PS; effect of salinity on adsorption of Pb^{2+} (c) and BPS (d) on β-CD-PS.

The subsequent experiment selected the original solution (pH = 5.44) for the study. When pH was between 2 and 7, the adsorption capacity of BPS basically did not change, when pH > 7, the adsorption capacity decreased significantly. This may be because under acidic conditions, the hydroxyl group on β-CD forms a hydrogen bond with the hydroxyl group on BPS, with the help of hydrogen bond, it was more conducive for BPS to reach the wide mouth end and enter the β-CD cavity through hydrophobic action. When pH was relatively high, the presence of OH^- in the solution hinders the formation of hydrogen bond, resulting in the decrease of adsorption capacity. Considering the practical application, BPS stock solution (pH = 5.96) was selected for the follow-up experiment.

3.2.4. Effect of common salts on adsorption

It was necessary to study the effect of coexisted salt in solution on adsorption quantity as there were common salts in dye wastewater. The results of effect of common salts are shown in Fig. 3c and d. The presence of salt had a negative effect on Pb^{2+} adsorption, which may be due to the competitive adsorption of Na^+ and Ca^{2+} with Pb^{2+} in salt solution. The intense of competition is more at larger salt concentration, resulting in a decrease in adsorption capacity. With the increase of salt concentration, the adsorption capacity of BPS basically did not change, indicating that β-CD-PS has a good selectivity for the adsorption of BPS.

3.2.5. Adsorption isotherm

The effect of equilibrium Pb^{2+} and BPS concentration and solution temperature on adsorption quantity are performed and the results are presented in Figs. 4a and 5a. When the concentration was relatively lower, the adsorption capacity increased with the increase of the concentration of Pb^{2+}. This was because the concentration increased resulting in the concentration gradient of β-CD-PS surface increase, more Pb^{2+} was bound to the adsorbent surface. When the equilibrium concentration was greater than 20 mg·L^{-1}, with the increase of the concentration of Pb^{2+}, the adsorption amount remained unchanged and the adsorption equilibrium was reached, the active sited on β-CD-PS were all bound to the adsorbate, and the adsorbent was saturated. When Pb^{2+} concentration was 200 mg·L^{-1}, the equilibrium adsorption capacity at 293, 303 and 313 K was 89.6, 93.0 and 97.4 mg·g^{-1}, respectively. With the increase of temperature, the adsorption capacity increased. The adsorption of Pb^{2+} was an endothermic process. As could be seen from Fig. 5a for BPS adsorption, at the same temperature, the adsorption capacity increased with the increase of concentration, and at the same concentration, the adsorption capacity was inversely proportional to the temperature, indicating that the adsorption of β-CD-PS to BPS was an exothermic process, and the increase of temperature reduces the active sited on the surface of β-CD-PS. Similar results were found in other studies [45].

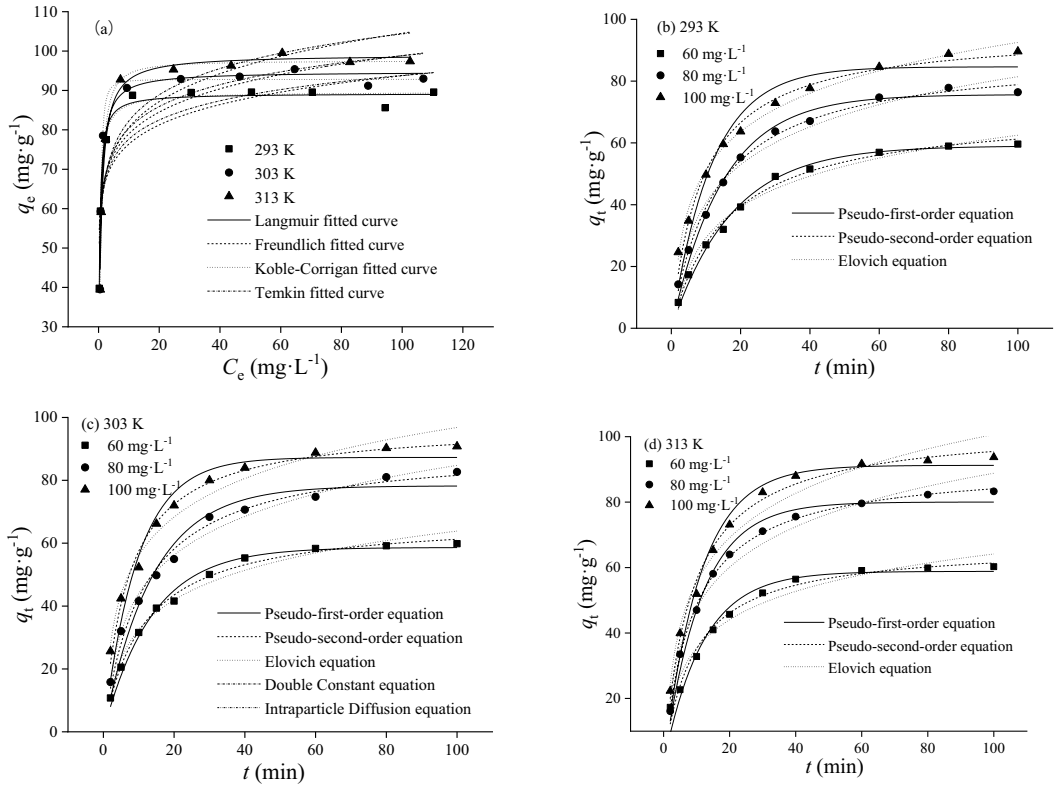

Fig. 4. Adsorption isotherms of Pb^{2+} (a); kinetic curve of Pb^{2+} adsorption (b) 293 K, (c) 303 K, and (d) 313 K.

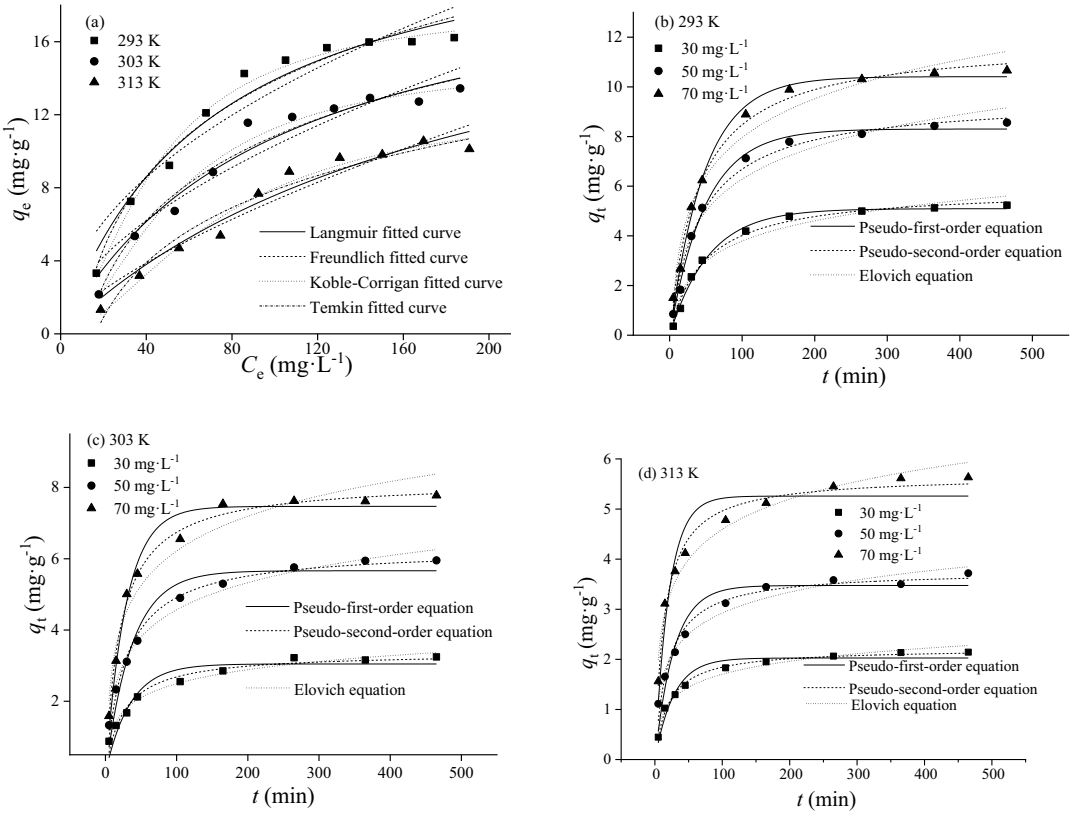

Fig. 5. Adsorption isotherms of BPS (a); kinetic curves of BPS adsorption (b) 293 K, (c) 303 k, and (d) 313 K.

Table 1
Adsorption model applied in this study

Adsorption model	Expression	Parameters
	Isotherm models	
Langmuir model	$q_e = \frac{q_m K_L C_e}{1 + K_L C_e}$	q_m or q_e (mg·g^{-1}) is the maximum or equilibrium adsorption capacity; K_L (L·mg^{-1}) is related to the adsorption affinity of the binding energy
Freundlich model	$q_e = K_F C_e^{1/n}$	K_F is the Freundlich constant related to the comparative adsorption capacity; $1/n$ is the affinity of the adsorbate
Temkin equation	$q_e = A_T + B_T \ln C_e$	A_T and B_T are the constants of the Temkin isotherm
Koble–Corrigan model	$q_e = \frac{AC_e^n}{1 + BC_e^n}$	A and B are the constants of the Koble–Corrigan model
	Kinetic models	
Pseudo-first-order kinetic model	$q_t = q_e\left(1 - e^{-k_1 t}\right)$	k_1 is the rate constant (min^{-1})
Pseudo-second-order kinetic model	$q_t = \frac{k_2 q_e^2 t}{1 + k_2 q_e t}$	k_2 (g·mg^{-1}·min^{-1}) is the reaction rate coefficient of pseudo-second-order kinetic model
Elovich equation	$q_t = A + B\ln t$	A and B are parameters of this model

The equilibrium data can be analyzed to study the adsorption mechanism, the maximum adsorption capacity, and the properties of the adsorbent. In this experiment, four common models, Langmuir, Freundlich, Temkin and Koble–Corrigan are selected and the expressions of models are shown in Table 1. The fitting results are presented in Table 2 (for Pb^{2+}) and Table 3 (for BPS) while the fitted curves are also shown in Figs. 4a and 5a, respectively.

Table 2 shows the isotherm model fitting results for Pb^{2+} adsorption. From the fitting results, it could be seen that the values of $q_{e(\exp)}$ and $q_{m(\text{theo})}$ in the Langmuir model were very close and could be used to predict the unit adsorption of Pb^{2+}, and the R^2 values were large, 0.989, 0.948 and 0.983, respectively, and the SSE values were smaller. This indicated that the adsorption of Pb^{2+} on β-CD-PS was a single molecular layer adsorption. Compared to the other models, the R^2 values of Freundlich and Temkin models were smaller while the SSE values were larger. This showed that Freundlich model and Temkin model were not suitable for describing this adsorption process. The value of the parameter n in the Koble–Corrigan model tended to be close to 1. This indicated that the Koble–Corrigan model was more inclined to the Langmuir model, and the determined coefficients R^2 in the fitting results were the highest among these four models (0.989, 0991, and 0.990 at three temperatures, respectively), and the values of SSE were the smallest among the four models. Combining the close between fitted curves and experimental curves, the Koble–Corrigan model could be used to describe the adsorption process of β-CD-PS toward Pb^{2+}.

For BPS, it could be seen from Table 3 that the K_L value decreases from 14.1 to 5.07 L·mg^{-1} as the temperature increased from 293 to 313 K. The lower the temperature,

Table 2
Parameters of adsorption isotherm models for Pb^{2+} adsorption onto β-CD-PS

Langmuir					
T (K)	$q_{e(\exp)}$ (mg·g^{-1})	$q_{m(\text{theo})}$ (mg·g^{-1})	K_L (L·mg^{-1})	R^2	SSE
293	89.6	89.2 ± 0.76	3.31 ± 0.22	0.989	24.2
303	93.0	94.8 ± 1.9	2.06 ± 0.28	0.948	139
313	97.4	99.1 ± 1.2	1.46 ± 0.12	0.983	52.8
Freundlich					
T (K)	$q_{e(\exp)}$ (mg·g^{-1})	K_F	$1/n \times 10^{-2}$	R^2	SSE
293	89.6	62.2 ± 4.7	8.89 ± 2.1	0.741	569
303	93.0	63.1 ± 5.7	9.74 ± 2.5	0.693	818
313	97.4	62.2 ± 5.7	11.3 ± 2.5	0.747	795
Temkin					
T (K)	$q_{e(\exp)}$ (mg·g^{-1})	A_T	B_T	R^2	SSE
293	89.6	61.5 ± 4.0	7.02 ± 1.2	0.802	435
303	93.0	62.0 ± 5.2	8.01 ± 1.6	0.743	684
313	97.4	60.1 ± 5.1	9.60 ± 1.6	0.806	609
Koble–Corrigan					
T (K)	A	B	n	R^2	SSE
293	273 ± 29	3.05 ± 0.35	0.920 ± 0.089	0.989	21.3
303	276 ± 26	2.97 ± 0.29	1.87 ± 0.17	0.991	20.1
313	152 ± 10	1.56 ± 0.11	1.26 ± 0.12	0.990	28.3

Note: SSE = $\sum\left(q_c - q\right)^2$, q and q_c are the experimental value and calculated value according the model, respectively.

Table 3
Parameters of adsorption isotherm models for BPS adsorption onto β-CD-PS

Langmuir					
T (K)	$q_{e(\exp)}$ (mg·g^{-1})	$q_{m(\text{theo})}$ (mg·g^{-1})	K_L (L·mg^{-1})	R^2	SSE
293	16.2	23.8 ± 1.8	14.1 ± 2.6	0.963	5.92
303	13.4	21.5 ± 2.4	9.98 ± 2.40	0.953	5.62
313	10.1	22.5 ± 4.4	5.07 ± 1.60	0.955	3.82
Freundlich					
T (K)	$q_{e(\exp)}$ (mg·g^{-1})	K_F	$1/n$	R^2	SSE
293	16.2	1.44 ± 0.47	0.483 ± 0.067	0.867	16.5
303	13.4	0.801 ± 0.301	0.555 ± 0.077	0.902	11.6
313	10.1	0.302 ± 0.124	0.692 ± 0.084	0.928	6.12
Temkin					
T (K)	$q_{e(\exp)}$ (mg·g^{-1})	A_T	B_T	R^2	SSE
293	16.2	–12.5 ± 1.6	5.74 ± 0.35	0.967	5.32
303	13.4	–12.5 ± 1.4	5.06 ± 0.32	0.964	4.27
313	10.1	–12.1 ± 1.4	4.34 ± 0.32	0.954	3.94
Koble–Corrigan					
T (K)	$A \times 10^{-2}$	$B \times 10^{-3}$	n	R^2	SSE
293	3.72 ± 2.50	2.05 ± 1.30	1.64 ± 0.19	0.987	1.86
303	1.71 ± 1.81	1.13 ± 1.10	1.71 ± 0.28	0.976	2.51
313	0.794 ± 1.011	0.615 ± 0.740	1.71 ± 0.33	0.973	2.03

the larger the K_L value and the stronger the binding force, which was also consistent with the experimental results. The R^2 values for the three temperatures were above 0.95, but the difference between $q_{e(\exp)}$ and $q_{m(\text{theo})}$ was large, so the Langmuir model was not applicable to describe the adsorption process of BPS on β-CD-PS. The values of R^2 from the Freundlich model were small relative to the other models, and the SSE was large, indicating that it was also not applicable to describe the adsorption. The values of R^2 from the Temkin model and Koble–Corrigan model were larger while the values of SSE were smaller. The fitted curves from both models were closer to experimental curves. This confirmed that the Temkin model and Koble–Corrigan model were more suitable to describe the adsorption process of β-CD-PS toward BPS.

3.2.6. Adsorption kinetic study

The results at various contact time are shown in Fig. 4b–d for Pb^{2+} and Fig. 5b–d for BPS, respectively. As can be seen from Fig. 4b, the equilibrium adsorption amounts of β-CD-PS toward Pb^{2+} at 293 K were 59.6, 76.4, and 89.6 mg·g^{-1} for Pb^{2+} solution concentrations of 60, 80, and 100 mg·L^{-1}, respectively. From Fig. 4b–d it can be seen that the adsorption of Pb^{2+} on β-CD-PS was a fast adsorption process, and the adsorption amount of Pb^{2+} on β-CD-PS has reached more than 90% of the equilibrium adsorption amount at the adsorption time of 40 min. From Fig. 5b–d it can be seen that the adsorption of β-CD-PS toward BPS could be divided into three stages, taking Fig. 5b as an example, 0~45 min was the fast adsorption stage, 45~265 min was the medium adsorption stage, and 265~465 min was the slow adsorption until equilibrium was reached. This was because in the initial adsorption stage, the concentration gradient difference between the adsorbent and adsorbent was relatively large and the adsorption rate was fast. As time increases, the active sited on the surface of β-CD-PS were gradually occupied by BPS, and the concentration difference between the adsorbent and the adsorbent surface decreases, and the adsorption rate decreases until equilibrium is reached. From Figs. 4 and 5 it can be seen that the adsorption equilibrium time of Pb^{2+} and BPS on β-CD-PS was very different, and the adsorption of Pb^{2+} was basically saturated at 60 min, while the basic adsorption equilibrium of BPS was only at 300 min, which may be due to the direct complexation of Pb^{2+} with the carboxyl group on β-CD-PS, and the adsorption rate was relatively fast. For BPS adsorption, there was a host-guest interaction between BPS and β-CD, which takes some time to enter the inside of the β-CD cavity and the adsorption rate is slower.

Three common kinetic models (pseudo-first-order equation, pseudo-second-order equation, Elovich equation) are applied for fitting kinetic data, and the expressions of models are also shown in Table 1. The fitted curves are shown in Figs. 4 and 5, and the fitted parameters are shown in Table 4 (for Pb^{2+}) and Table 5 (for BPS), respectively.

As could be seen from the fitted data in Table 4 (for Pb^{2+}), the results of fitting the pseudo-first-order equation emerged that the $q_{e(\exp)}$ and $q_{e(\text{theo})}$ values were close to each other, and this result indicated that the pseudo-first-order equation to predict the unit adsorption and the R^2 values were all above 0.932 with small SSE values. Furthermore, the fitted curves from this model were closer to experimental curves. This confirmed that pseudo-first-order equation was suitable for describing the kinetic process. The values of R^2 from the pseudo-second-order equation were all above 0.980 and the values of SSE were smaller. But the difference between the $q_{e(\exp)}$ and $q_{e(\text{theo})}$ values in the fitted results was large. This shows that this model is suitable for describing the kinetic process and not proper to predict the adsorption quantity. The R^2 values from the Elovich equation were above 0.964 and the SSE values were small, indicating that this model can be used to predict the kinetic process and there was ion-exchange in the adsorption process.

From the fitted data in Table 5 (for BPS), it also could be obtained that the $q_{e(\exp)}$ and $q_{e(\text{theo})}$ values were relatively close in the fitted results of the pseudo-first-order equation, which proved that the pseudo-first-order equation to predict the unit adsorption, but the R^2 value was slightly small and not suitable for describing the adsorption process. The difference between $q_{e(\exp)}$ from experiments and $q_{e(\text{theo})}$ from pseudo-second-order equation was not significant, while the values of R^2 were above 0.970 and the values of SSE were smaller. So it was implied that pseudo-second-order equation was more suitable for describing the adsorption process, indicating that chemisorption was the main role. According to values of R^2 and SSE from Elovich equation, it was not better to fit the kinetic process.

Table 4
Adsorption kinetics fitting parameters of β-CD-PS for Pb^{2+}

Pseudo-first-order equation						
T (K)	C_0 (mg·L^{-1})	$q_{e(exp)}$ (mg·g^{-1})	$q_{e(theo)}$ (mg·g^{-1})	$k_1 \times 10^{-2}$	R^2	SSE
293	60	59.6	59.0 ± 1.0	5.72 ± 0.30	0.992	21.0
	80	76.4	75.6 ± 1.6	6.68 ± 0.45	0.985	59.4
	100	89.6	84.6 ± 3.1	8.50 ± 1.10	0.932	279
303	60	59.8	58.6 ± 1.1	7.28 ± 0.48	0.986	34.3
	80	82.7	78.2 ± 2.6	7.23 ± 0.79	0.957	172
	100	90.8	87.3 ± 2.5	10.3 ± 1.2	0.946	217
313	60	60.3	58.8 ± 1.7	8.44 ± 0.88	0.957	87.2
	80	83.3	80.0 ± 1.5	8.87 ± 0.61	0.983	71.5
	100	93.7	91.2 ± 2.1	9.02 ± 0.75	0.973	133
Pseudo-second-order equation						
T (K)	C_0 (mg·L^{-1})	$q_{e(exp)}$ (mg·g^{-1})	$q_{e(theo)}$ (mg·g^{-1})	$k_2 \times 10^{-4}$	R^2	SSE
293	60	59.6	71.0 ± 1.6	8.87 ± 0.83	0.993	18.1
	80	76.4	88.9 ± 1.6	8.85 ± 0.70	0.994	23.2
	100	89.6	96.4 ± 2.3	11.6 ± 1.4	0.983	68.5
303	60	59.8	68.2 ± 1.1	12.9 ± 0.97	0.995	12.7
	80	82.7	90.7 ± 2.2	9.80 ± 1.10	0.988	47.9
	100	90.8	97.9 ± 1.8	14.5 ± 1.4	0.988	48.4
313	60	60.3	66.9 ± 1.8	16.6 ± 2.2	0.980	10.8
	80	83.3	91.5 ± 0.6	12.3 ± 0.4	0.999	5.01
	100	93.7	104 ± 2	11.5 ± 1.0	0.991	43.0
Elovich equation						
T (K)	C_0 (mg·L^{-1})	A		B	R^2	SSE
293	60	–3.98 ± 2.32		14.4 ± 0.7	0.979	57.2
	80	–0.180 ± 2.801		17.7 ± 0.8	0.979	82.7
	100	9.92 ± 2.01		17.9 ± 0.6	0.990	41.1
303	60	1.16 ± 2.23		13.6 ± 0.6	0.978	52.0
	80	3.13 ± 2.04		17.7 ± 0.6	0.989	42.4
	100	15.2 ± 3.3		17.7 ± 1.0	0.971	118
313	60	6.73 ± 2.66		12.5 ± 0.8	0.964	73.2
	80	6.66 ± 3.17		17.8 ± 0.9	0.976	98.3
	100	10.5 ± 4.0		19.6 ± 1.2	0.967	165

3.2.7. Thermodynamic parameters of adsorption

Thermodynamic parameters including enthalpy change ($\Delta H°$), Gibb's free energy change ($\Delta G°$) and entropy change ($\Delta S°$) estimated the effect of temperature on the adsorption of Pb^{2+} and BPS on β-CD-PS. They could be determined using the following equations:

$$K_c = \frac{C_{ad,e}}{C_e} \tag{5}$$

$$\Delta G° = -RT \ln K_c \tag{6}$$

$$\Delta G° = \Delta H° - T\Delta S° \tag{7}$$

$$\ln k_2 = \ln k_0 - \frac{E_a}{RT} \tag{8}$$

where K_c is the equilibrium constant and $C_{ad,e}$ (mg·L^{-1}) is the concentration of the adsorbate on the adsorbent; R is the ideal gas constant (8.314 J·mol^{-1}·K^{-1}), T (K) is the temperature of the reaction medium, k_2 is the pseudo-second-order rate constant, k_0 is the temperature independent factor.

The thermodynamic parameters calculated are listed in Table 6. As seen in Table 6, $\Delta G° < 0$, and $\Delta S° > 0$ for Pb^{2+} adsorption, indicating that the adsorption of Pb^{2+} by β-CD-PS was a spontaneous, entropically increasing heat adsorption reaction. The value of $\Delta H° < 84$ kJ·mol^{-1} and the value of E_a ranged from 5–40 kJ·mol^{-1}, so there was a physical effect of Pb^{2+} adsorption. The results in the kinetic curve fitting showed that the adsorption process was in accordance with the quasi-level kinetics and Elovich equation, so the adsorption of Pb^{2+} by β-CD-PS had both physical and chemical adsorption.

Table 5
Adsorption kinetics fitting parameters of β-CD-PS for BPS

Pseudo-first-order equation						
T (K)	C_0 (mg·L^{-1})	$q_{e(exp)}$ (mg·g^{-1})	$q_{e(theo)}$ (mg·g^{-1})	$k_1 \times 10^{-2}$	R^2	SSE
	30	5.23	5.09 ± 0.08	1.86 ± 0.10	0.994	14.2
293	50	8.56	8.30 ± 0.12	2.01 ± 0.11	0.994	38.2
	70	10.7	10.4 ± 0.15	2.07 ± 0.11	0.993	59.1
	30	3.25	3.05 ± 0.13	2.90 ± 0.50	0.903	53.1
303	50	5.96	5.66 ± 0.19	2.69 ± 0.36	0.946	111
	70	7.78	7.47 ± 0.17	3.44 ± 0.33	0.972	97.2
	30	2.14	2.03 ± 0.06	3.58 ± 0.45	0.949	12.3
313	50	3.72	3.47 ± 0.13	3.52 ± 0.56	0.906	58.3
	70	5.63	5.26 ± 0.19	4.77 ± 0.75	0.906	123
Pseudo-second-order equation						
T (K)	C_0 (mg·L^{-1})	$q_{e(exp)}$ (mg·g^{-1})	$q_{e(theo)}$ (mg·g^{-1})	$k_2 \times 10^{-3}$	R^2	SSE
	30	5.23	5.90 ± 0.17	3.60 ± 0.47	0.989	26.3
293	50	8.56	9.54 ± 0.26	2.45 ± 0.32	0.988	71.8
	70	10.7	11.9 ± 0.3	2.10 ± 0.21	0.993	64.0
	30	3.25	3.36 ± 0.11	11.7 ± 2.0	0.966	18.8
303	50	5.96	6.29 ± 0.13	5.67 ± 0.60	0.988	23.9
	70	7.78	8.19 ± 0.13	5.71 ± 0.49	0.992	27.9
	30	2.14	2.21 ± 0.027	22.4 ± 1.5	0.995	13.2
313	50	3.72	3.77 ± 0.10	13.7 ± 2.1	0.970	18.5
	70	5.63	5.67 ± 0.09	12.4 ± 1.3	0.985	19.2
Elovich equation						
T (K)	C_0 (mg·L^{-1})	A		B	R^2	SSE
	30	–1.63 ± 0.34		1.18 ± 0.07	0.970	72.6
293	50	–2.33 ± 0.59		1.87 ± 0.13	0.962	228
	70	–2.44 ± 0.70		2.26 ± 0.15	0.965	313
	30	–0.110 ± 0.012		0.566 ± 0.027	0.982	9.84
303	50	–0.487 ± 0.020		1.10 ± 0.044	0.987	26.2
	70	–0.246 ± 0.053		1.40 ± 0.12	0.948	181
	30	–0.184 ± 0.099		0.374 ± 0.022	0.974	6.35
313	50	0.148 ± 0.016		0.602 ± 0.035	0.974	16.3
	70	0.589 ± 0.260		0.870 ± 0.057	0.967	43.3

Table 6
Thermodynamic parameters and apparent activation energy of Pb^{2+} and BPS adsorption

Adsorbent	E_a (kJ·mol^{-1})	$\Delta H°$ (kJ·mol^{-1})	$\Delta S°$ (J·mol^{-1}·K^{-1})	$\Delta G°$ (kJ·mol^{-1})		
				293 K	303 K	313 K
Pb^{2+}	16.0	24.6	99.8	–5.13	–5.72	–6.64
BPS	69.9	–39.6	–149	–3.92	–5.32	–6.90

From the thermodynamic parameters and apparent activation energy of β-CD-PS toward BPS in Table 4, it could be seen that the adsorption of BPS was a spontaneous, entropy-decreasing exothermic reaction. Since the E_a value was to 69.9 kJ·mol^{-1}, there was chemisorption during adsorption process.

3.2.8. Desorption study

In order to explore whether the exhausted material could be recycled, the spent adsorbent can be desorbed or regenerated and this can improve the value of adsorbent. The methods for desorption and regeneration was selected for multiple desorption. The results are shown in Fig. 6.

From Fig. 6a it can be seen that 0.1 mol·L^{-1} HNO_3 has the best desorption effect on Pb^{2+} loaded β-CD-PS with 109% desorption rate and 55.6% regeneration rate. This may be because the presence of acid disrupted the force between Pb^{2+} and β-CD-PS, or ion-exchange between H^+ and Pb^{2+} desorbed it down. It was selected to be regenerated by desorption three times with 0.1 mol·L^{-1} HNO_3, and the results were shown in Fig. 6b. All three desorption rates were above 90% and regeneration rates were above 60%, indicating that the β-CD-PS adsorbed with Pb^{2+} had some cyclic regeneration ability. As can be seen from Fig. 6c, the best desorption and regeneration among these desorbents was 75% C_2H_5OH, whose desorption and regeneration rates were 94.4% and 73.9%, respectively. It was possible that the presence of ethanol weakened the binding force between the cavity interior of β-CD and BPS, and therefore desorbed down. The adsorbent was selected to be regenerated by multiple desorptions with 75% C_2H_5OH, as shown in Fig. 6d. As the number of desorptions increased, the desorption efficiency decreased, but all values of *d* were above 85% and the values of *r* were all above 75%, indicating that the BPS-loaded β-CD-PS could be utilized several times and had good regenerative properties.

3.2.9. X-ray photoelectron spectroscopy analysis and mechanism study

In this study, X-ray photoelectron spectroscopy (XPS) characterization analysis was performed before and after the adsorption of Pb^{2+} and BPS on β-CD-PS, and the adsorption mechanism was investigated. Its XPS full spectrum and O1s split peak diagram are shown in Fig. 7.

From the full spectra of Fig. 7a–c it can be seen that a Pb3d peak appeared at 138.97 eV in Fig. 7b, indicating the successful adsorption of Pb^{2+} on β-CD-PS, and an S3p peak appeared at 168.23 eV in Fig. 7c, indicating the successful adsorption of BPS on β-CD-PS. The 532.91 and 531.05 eV in Fig. 7d1 were the –OH and C–O bonds, respectively, with the percentages of 88.94% and 11.06%; Fig. 7d2 shows that the binding energies of –OH and C–O bonds after adsorption of Pb^{2+} were 532.83 and 531.05 eV, respectively, with the percentages of 76.48% and 5.44%, respectively, and the decrease in the percentage of –OH may be due to the introduction of Pb^{2+} which reduces the binding of O to H Moreover, one peak of Pb–O appears at 533.99 eV, indicating the successful adsorption of Pb^{2+}; Fig. 7d3 shows that the binding energies of –OH and C–O bonds became 532.77 and 532.33 eV, respectively, after adsorption of BPS, with the percentages of 62.35% and 37.65%, with an increase in the percentage content of –OH, which may be caused by the formation of hydrogen bonds between β-CD and BPS or the introduction of BPS during the adsorption process, indicating that β-CD-PS effectively adsorbed BPS.

The isotherm and kinetic results showed that the force between β-CD-PS and Pb^{2+} was mainly the complexation of Pb^{2+} with the carboxyl group of CA on β-CD-PS along with ion-exchange. β-CD had a hydrophobic cavity structure, and BPS could enter the interior of the cavity through the

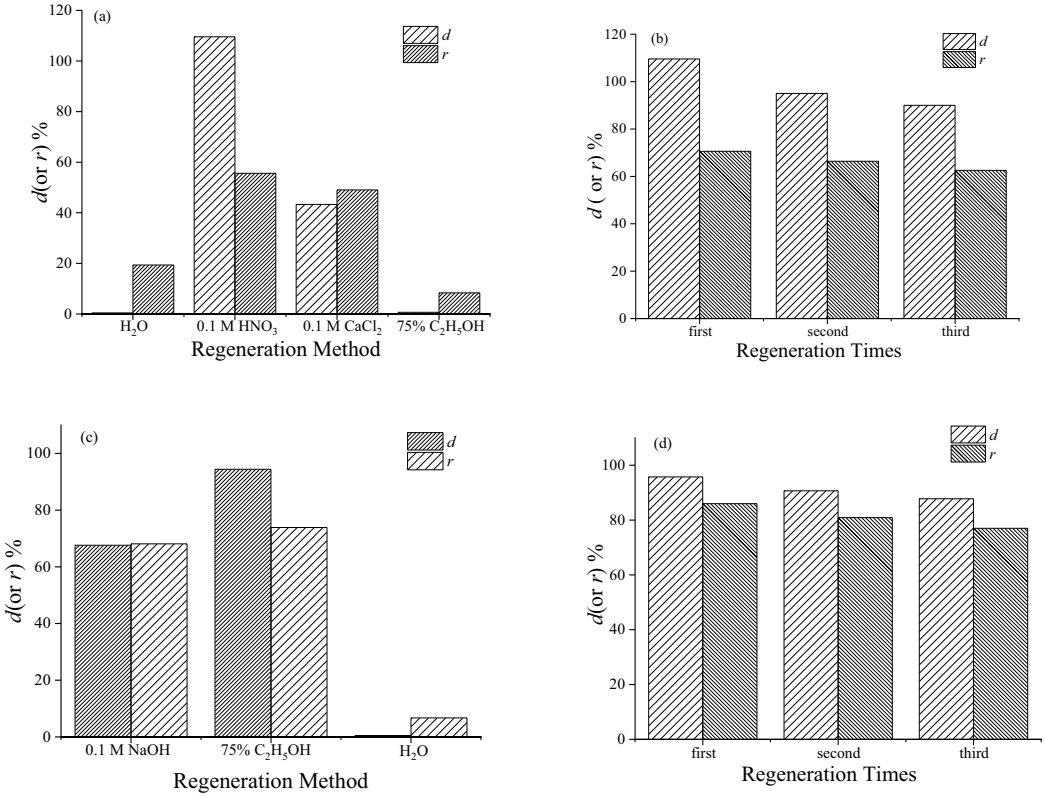

Fig. 6. (a) Desorption and regeneration effect after Pb^{2+} adsorption, (b) 0.1 mol·L^{-1} HNO_3 three times desorption regeneration for Pb^{2+}, (c) desorption and regeneration effect after BPS adsorption, and (d) 75% C_2H_5OH triple desorption regeneration for BPS.

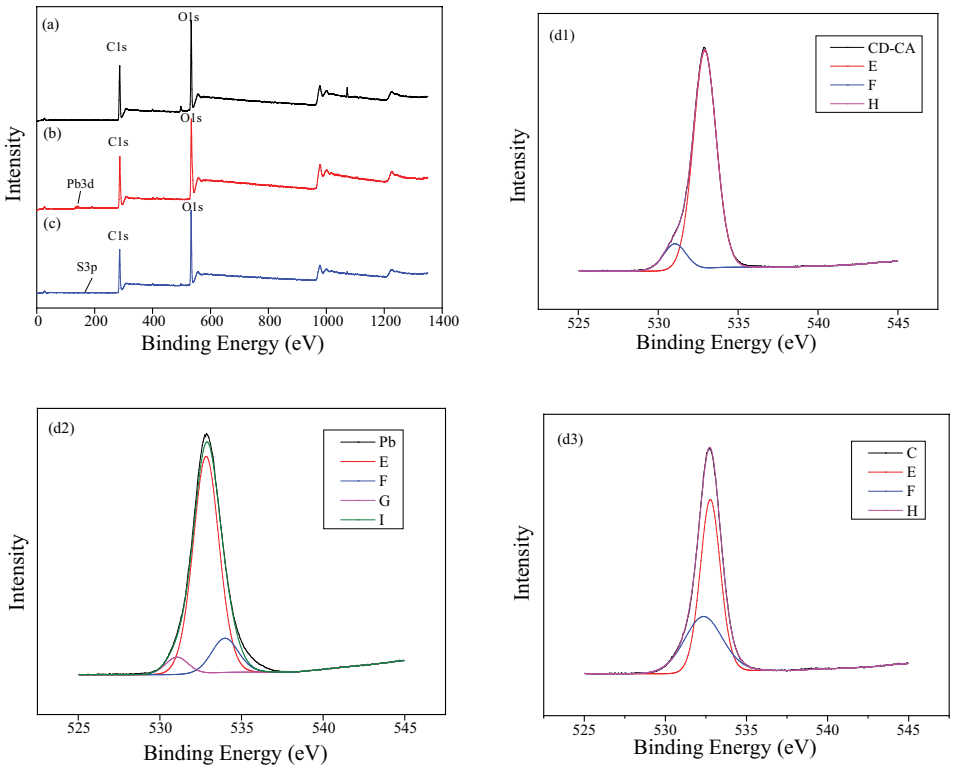

Fig. 7. X-ray photoelectron spectroscopy full spectra of β-CD-PS before and after Pb^{2+} and BPS adsorption (a) before adsorption, (b) after Pb^{2+} adsorption, (c) after BPS adsorption and O1s peak splitting (d1) before adsorption, (d2) after Pb^{2+} adsorption, and (d3) after BPS adsorption.

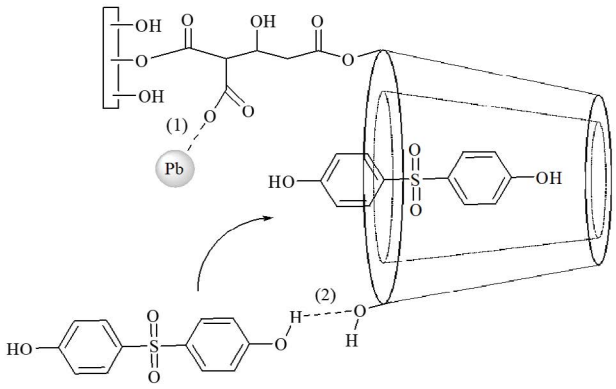

Fig. 8. Schematic diagram of the mechanism of interaction between β-CD-PS and Pb^{2+} and BPS: (1) complexation/ion-exchange and (2) hydrogen bonding.

wide-mouth end of β-CD. The –OH on BPS forms p-π conjugation system with the benzene ring so that the hydrogen on its –OH. The –OH on BPS forms a p-π conjugate system with the benzene ring so that the hydrogen on its –OH exhibits a positive charge, while the oxygen on the –OH in the β-CD exhibits a negative charge, so BPS can form a hydrogen bond with the β-CD, which was more favorable for BPS to enter the cavity. Fig. 8 shows the mechanism of interaction between β-CD-PS and Pb^{2+} and BPS.

4. Conclusions

The adsorption performance of both Pb^{2+} and BPS on β-CD-PS was significantly improved compared with that of natural peanut shell. Acidic conditions were not favorable for the adsorption of Pb^{2+}. The adsorption of BPS remained essentially constant at pH 2–7, and alkaline conditions were not favorable. The presence of salt was unfavorable to Pb^{2+} adsorption, but had no effect on BPS adsorption. The isotherm results showed that the Langmuir model and the Koble–Corrigan model could be used to describe the Pb^{2+} adsorption on β-CD-PS, and the Temkin model and the Koble–Corrigan model could well describe the adsorption process of BPS on β-CD-PS. The pseudo-first-order model and Elovich model could be used to describe the kinetic process of Pb^{2+} adsorption, indicating the existence of ion-exchange in the adsorption process. The adsorption process of β-CD-PS toward BPS was consistent with the pseudo-second-order model, suggesting that chemisorption be the main rate-controlling step. The Pb^{2+} adsorption on β-CD-PS was a spontaneous, entropy-increasing, heat-absorbing reaction while BPS adsorption on β-CD-PS was a spontaneous, entropy-decreasing, exothermic reaction. Pb^{2+} or BPS-loaded β-CD-PS can be regenerated and reused. There is potential for β-CD-PS to remediate wastewater containing lead ion and BPS. This study provides one way to effectively utilize the agricultural by-product (such as peanut husk) for remediation of wastewater.

Acknowledgements

This work was financially supported by the Henan Province basis and advancing technology research project (142300410224).

References

[1] A. Issakhov, A. Alimbek, Y. Zhandaulet, The assessment of water pollution by chemical reaction products from the activities of industrial facilities: numerical study, J. Cleaner Prod., 282 (2021) 125239, doi: 10.1016/j.jclepro.2020.125239.
[2] N. Yuan, X.R. Gong, W.D. Sun, C.H. Yu, Advanced applications of Zr-based MOFs in the removal of water pollutants, Chemosphere, 267 (2021) 128863, doi: 10.1016/j.chemosphere.2020.128863.
[3] G. Crini, E. Lichtfouse, Advantages and disadvantages of techniques used for wastewater treatment, Environ. Chem. Lett., 17 (2018) 145–155.
[4] S. Kaushal, N. Kaur, M. Kaur, P.P. Singh, Dual-responsive pectin/graphene oxide (Pc/GO) nano-composite as an efficient adsorbent for Cr(III) ions and photocatalyst for degradation of organic dyes in waste water, J. Photochem. Photobiol. A, 403 (2020) 112841, doi: 10.1016/j.jphotochem.2020.112841.
[5] S.T. Zhuang, X. Zhu, J.L. Wang, Adsorptive removal of plasticizer (dimethyl phthalate) and antibiotic (sulfamethazine) from municipal wastewater by magnetic carbon nanotubes, J. Mol. Liq., 319 (2020) 114267, doi: 10.1016/j.molliq.2020.114267.
[6] A. Eman, F. Alakhras, L. Anastopoulos, D. Das, A. Al-Arfaj, N. Ouerfelli, A. Hosseini-Bandegharaei, Chitosan-based materials for the removal of nickel ions from aqueous solutions, Russ. J. Phys. Chem. A, 94 (2020) 748–755.
[7] G.B. Gerber, A. Léonard, Ph. Hantson, Carcinogenicity, mutagenicity and teratogenicity of manganese, Crit. Rev. Oncol./Hematol., 42 (2002) 25–34.
[8] M. Amjad, M.M. Iqbal, G. Abbas, A.B.U. Farooq, M.A. Naeem, M. Imran, B. Murtaza, M. Nadeem, S.E. Jacobsen, Assessment of cadmium and lead tolerance potential of quinoa (*Chenopodium quinoa* Willd) and its implications for phytoremediation and human health, Environ. Geochem. Health, 44 (2022) 1487–1500.
[9] N. Li, Y. Kang, W.J. Pan, L.X. Zeng, Q.Y. Zhang, J.W. Luo, Concentration and transportation of heavy metals in vegetables and risk assessment of human exposure to bioaccessible heavy metals in soil near a waste-incinerator site, South China, Sci. Total Environ., 521–522 (2015) 144–151.
[10] E.P. Puglla, D. Guaya, C. Tituana, F. Osorio, M.J. García-Ruiz, Biochar from agricultural by-products for the removal of lead and cadmium from drinking water, Water, 12 (2020) 2933, doi: 10.3390/w12102933.
[11] Y.J. Chen, M. He, B.B. Chen, B. Hu, Thiol-grafted magnetic polymer for preconcentration of Cd, Hg, Pb from environmental water followed by inductively coupled plasma mass spectrometry detection, Spectrochim. Acta, Part B, 177 (2021) 106071, doi: 10.1016/j.sab.2021.106071.
[12] A.K. Sonker, M. Bhateria, K. Karsauliya, S.P. Singh, Investigating the glucuronidation and sulfation pathways contribution and disposition kinetics of bisphenol S and its metabolites using LC-MS/MS-based nonenzymatic hydrolysis method, Chemosphere, 273 (2021) 129624, doi: 10.1016/j.chemosphere.2021.129624.
[13] S.Q. Zhang, J.-Q. Jiang, M. Petri, Preliminarily comparative performance of removing bisphenol-S by ferrate oxidation and ozonation, npj Clean Water, 4 (2021) 1, doi: 10.1038/s41545-020-00095-x.
[14] A. Salahinejad, A. Attaran, M. Naderi, D. Meuthen, S. Niyogi, D.P. Chivers, Chronic exposure to bisphenol S induces oxidative stress, abnormal anxiety, and fear responses in adult zebrafish (*Danio rerio*), Sci. Total Environ., 750 (2021) 141633, doi: 10.1016/j.scitotenv.2020.141633.
[15] T.D. Ding, W. Li, M.T. Yang, B. Yang, J.Y. Li, Toxicity and biotransformation of bisphenol S in freshwater green alga *Chlorella vulgaris*, Sci. Total Environ., 747 (2020) 141144, doi: 10.1016/j.scitotenv.2020.141144.
[16] M. Naderi, M.Y. Wong, F. Gholami, Developmental exposure of zebrafish (*Danio rerio*) to bisphenol-S impairs subsequent reproduction potential and hormonal balance in adults, Aquat. Toxicol., 148 (2014) 195–203.
[17] W.X. Liu, F. Donatella, S.J. Tan, W. Ge, J.J. Wang, X.F. Sun, S.F. Cheng, W. Shen, Detrimental effect of bisphenol S in mouse germ cell cyst breakdown and primordial follicle assembly, Chemosphere, 264 (2021) 128445, doi: 10.1016/j.chemosphere.2020.128445.
[18] Q. Lin, Y.Y. Wu, F.C. Lin, X. Liu, B.L. Lu, Removal of bisphenol A from aqueous solution via host-guest interactions based on beta-cyclodextrin grafted cellulose bead, Int. J. Biol. Macromol., 140 (2019) 1–9.
[19] Q.M. Liu, Y. Zhou, J. Lu, Y.B. Zhou, Novel cyclodextrin-based adsorbents for removing pollutants from wastewater: a critical review, Chemosphere, 241 (2020) 125043, doi: 10.1016/j.chemosphere.2019.125043.
[20] B. Gidwani, A. Vyas, Synthesis, characterization and application of epichlorohydrin-β-cyclodextrin polymer, Colloids Surf., B, 114 (2014) 130–137.
[21] Y.B. Zhou, G. Cheng, K. Chen, J. Lu, J.Y. Lei, S.Y. Pu, Adsorptive removal of bisphenol A, chloroxylenol, and carbamazepine from water using a novel beta-cyclodextrin polymer, Ecotoxicol. Environ. Saf., 170 (2019) 278–285.
[22] A.J. Méndez-Martínez, M.M. Dávila-Jiménez, O. Ornelas-Dávila, M.P. Elizalde-González, U. Arroyo-Abad, I. Sirés, E. Brillas, Electrochemical reduction and oxidation pathways for Reactive Black 5 dye using nickel electrodes in divided and undivided cells, Electrochim. Acta, 59 (2012) 140–149.
[23] A. Dabrowski, P. Podkoscielny, Z. Hubicki, M. Barczak, Adsorption of phenolic compounds by activated carbon – a critical review, Chemosphere, 58 (2005) 1049–1070.
[24] M.E. Avval, P.N. Moghadam, M.M. Baradarani, Synthesis of a new nanocomposite based on graphene oxide for selective removal of Pb^{2+} ions from aqueous solutions, Polym. Compos., 40 (2018) 730–737.
[25] M. Petersková, C. Valderrama, O. Gibert, J.L. Cortina, Extraction of valuable metal ions (Cs, Rb, Li, U) from reverse osmosis concentrate using selective sorbents, Desalination, 286 (2012) 316–323.
[26] B.A.M. Al-Rashdi, D.J. Johnson, N. Hilal, Removal of heavy metal ions by nanofiltration, Desalination, 315 (2013) 2–17.
[27] D. Elenter, K. Milferstedt, W. Zhang, M. Hausner, E. Morgenroth, Influence of detachment on substrate removal and microbial ecology in a heterotrophic/autotrophic biofilm, Water Res., 41 (2007) 4657–4671.
[28] L. Niazi, A. Lashanizadegan, H. Sharififard, Chestnut oak shells activated carbon: preparation, characterization and application for Cr(VI) removal from dilute aqueous solutions, J. Cleaner Prod., 185 (2018) 554–561.
[29] F.L. Mi, S.J. Wu, F.M. Lin, Adsorption of copper(II) ions by a chitosan-oxalate complex biosorbent, Int. J. Biol. Macromol., 72 (2015) 136–144.
[30] X. Xu, B.Y. Gao, B. Jin, Q.Y. Yue, Removal of anionic pollutants from liquids by biomass materials: a review, J. Mol. Liq., 215 (2016) 565–595.
[31] D. Wei, Z.S. Chen, J. Jin, B.B. Wei, Q. Li, S.Y. Yang, Z.M. Yu, A. Alsaedi, T. Hayat, X.K. Wang, Interaction of U(VI) with amine-modified peanut shell studied by macroscopic and microscopic spectroscopy analysis, J. Cleaner Prod., 195 (2018) 497–506.
[32] J.J. Dong, Y.Y. Du, R.S. Duyu, Y. Shang, S.S. Zhang, R.P. Han, Adsorption of copper ion from solution by polyethylenimine modified wheat straw, Bioresour. Technol. Rep., 6 (2019) 96–102.
[33] R.P. Han, D.D. Ding, Y.F. Xu, W.H. Zou, Y.F. Wang, Y.F. Li, L. Zou, Use of rice husk for the adsorption of Congo red from aqueous solution in column mode, Bioresour. Technol., 99 (2008) 2938–2946.
[34] O.C. Iheanacho, J.T. Nwabanne, C.C. Obi, C.E. Onu, Packed bed column adsorption of phenol onto corn cob activated carbon:

linear and nonlinear kinetics modeling, S. Afr. J. Chem. Eng., 36 (2021) 80–93.
[35] P. Dan, S.P. Cheng, H.S. Li, X.T. Guo, Effective multi-functional biosorbent derived from corn stalk pith for dyes and oils removal, Chemosphere, 272 (2021) 129963, doi: 10.1016/j.chemosphere.2021.129963.
[36] F.M. Mpatani, A.A. Aryee, A.N. Kani, Q.H. Guo, E. Dovi, L.B. Qu, Z.H. Li, R.P. Han, Uptake of micropollutant-bisphenol A, methylene blue and neutral red onto a novel bagasse-β-cyclodextrin polymer by adsorption process, Chemosphere, 259 (2020) 127439, doi: 10.1016/j.chemosphere.2020.127439.
[37] M.Y. Liu, X.Y. Li, Y.Y. Du, R.P. Han, Adsorption of methyl blue from solution using walnut shell and reuse in a secondary adsorption for Congo red, Bioresour. Technol. Rep., 5 (2019) 238–242.
[38] A.A. Aryee, F.M. Mpatani, Y.Y. Du, A.N. Kani, E. Dovi, R.P. Han, Z.H. Li, L.B. Qu, Fe_3O_4 and iminodiacetic acid modified peanut husk as a novel adsorbent for the uptake of Cu(II) and Pb(II) in aqueous solution: characterization, equilibrium and kinetic study, Environ. Pollut., 268 (2021) 115729, doi: 10.1016/j.envpol.2020.115729.
[39] N.B. Singh, Y.K. Srivastava, S.P. Shukla, Markandeya, Investigating the efficacy of saw dust in fluoride removal through adsorption, J. Inst. Eng. India Ser. A, 100 (2019) 667–674.
[40] R.P. Han, W.H. Zou, W.H. Yu, S.J. Cheng, Y.F. Wang, J. Shi, Biosorption of methylene blue from aqueous solution by fallen phoenix tree's leaves, J. Hazard. Mater., 141 (2007) 156–162.
[41] C. Saka, Ö. Şahin, M.M. Küçük, Applications on agricultural and forest waste adsorbents for the removal of lead(II) from contaminated waters, Int. J. Environ. Sci. Technol., 9 (2012) 379–394.
[42] B.L. Zhao, Y. Shang, W. Xiao, C.C. Dou, R.P. Han, Adsorption of Congo red from solution using cationic surfactant modified wheat straw in column model, J. Environ. Chem. Eng., 2 (2014) 40–45.
[43] A. Hashem, C.O. Aniagor, M.F. Nasr, A. Abou-Okeil, Efficacy of treated sodium alginate and activated carbon fibre for Pb(II) adsorption, Int. J. Biol. Macromol., 176 (2021) 201–216.
[44] Y.C. Lv, J.C. Ma, K.Y. Liu, Y.T. Jiang, G.F. Yang, Y.F. Liu, C.X. Lin, X.X. Ye, Y.Q. Shi, M.H. Liu, L.H. Li, Rapid elimination of trace bisphenol pollutants with porous β-cyclodextrin modified cellulose nanofibrous membrane in water: adsorption behavior and mechanism, J. Hazard. Mater., 403 (2021) 123666, doi: 10.1016/j.jhazmat.2020.123666.
[45] N. Goyal, S. Barman, V.K. Bulasara, Efficient removal of bisphenol S from aqueous solution by synthesized nano-zeolite secony mobil-5, Microporous Mesoporous Mater., 259 (2018) 184–194.